Separation of particles leading either to decay or unlimited growth of energy in a driven stadium-like billiard

2014 J. Phys. A: Math. Theor. 47 365101

(http://iopscience.iop.org/1751-8121/47/36/365101)

IOP Publishing Journal of Physics A: Mathematical and Theoretical
J. Phys. A: Math. Theor **47** (2014) 365101 (17pp) doi:10.1088/1751-8113/47/36/365101

Separation of particles leading either to decay or unlimited growth of energy in a driven stadium-like billiard

André L P Livorati[1,2], Matheus S Palmero[2,3], Carl P Dettmann[2], Iberê L Caldas[1] and Edson D Leonel[3]

[1] Instituto de Física (IFUSP), Universidade de São Paulo (USP), Rua do Matão Tr.R 187, Cidade Universitária, 05314-970, São Paulo SP, Brazil
[2] School of Mathematics, University of Bristol, Bristol BS8 1TW, UK
[3] Departamento de Física (UNESP), Universidade Estadual Paulista, Av. 24A 1515, Bela Vista, 13506-900, Rio Claro, SP, Brazil

E-mail: livorati@usp.br and andrelivorati@gmail.com

Received 18 March 2014, revised 16 July 2014
Accepted for publication 18 July 2014
Published 22 August 2014

Abstract

Competition between the decay and growth of energy in a time-dependent stadium billiard is discussed with emphasis on the decay of the energy mechanism. A critical resonance velocity is identified as causing the separation between ensembles of high and low energy and a statistical investigation is performed using ensembles of initial conditions both above and below the resonance velocity. For high initial velocity, Fermi acceleration is inherent in the system. However, for low initial velocity, the resonance and stickiness hold the particles in a regular or quasi-regular regime near the fixed points, preventing them from exhibiting Fermi acceleration. Also, a transport analysis along the velocity axis is discussed to quantify the competition in the growth and decay of the energy, making use of the distributions of histograms of frequency, and we find that the energy decay is caused by the capture of the orbits by the resonant fixed points.

Keywords: Chaos, stadium billiard, stickiness, Fermi accleration
PACS numbers: 05.45.-a, 05.45.Pq, 05.45.Tp

(Some figures may appear in colour only in the online journal)

1. Introduction

Modelling dynamical systems with mixed phase space has been one of the main challenges of the research field of non-linear statistical mechanics and has especially received attention in the last few decades [1–4]. In particular, with the advances in fast computers, the dynamics can now be evolved over long time series, allowing several phenomena, some of them completely new, to be observed. The class of dynamics of particular interest include Hamiltonian systems with time-dependent perturbation, for which energy varies with time. Moreover, a better understanding of the mixed dynamics in phase space can be given and phenomena related to them can be carefully characterized. The study of the chaotic properties of systems can be found in many fields of physics such as fluids [5], plasmas [6, 7], nanotubes [8] and complex networks [9]. Interesting applications and phenomena can be found in optics [10–12] and acoustics [13] if billiard dynamics is considered. If the billiard boundaries are time dependent, applications in microwaves [14–16] and quantum dots [17–20] can also be found. Also, when a particle–particle iteration in billiard dynamics is considered, one can find synchronization [21, 22] and soft wall effects [23, 24].

A specific phenomenon which intrigues physicists in general is the unlimited energy growth of a bouncing particle with a driven boundary, a phenomenon called Fermi acceleration (FA). It was introduced in 1949 by Enrico Fermi [25] as an attempt to describe the mechanism in which particles that have their origin in cosmic rays acquire very high energy. His idea has now been extended to other models where the average properties of the velocity or kinetic energy for long time series are studied. In light of this approach, a billiard type dynamics is one of the most useful systems [26] which possibly exhibits unlimited energy growth when the boundary is moving in time. The Loskutov–Ryabov–Akinshin (LRA) conjecture then gives the minimal conditions to observe such a phenomenon [27, 28]. It claims that if a billiard has a chaotic component for the dynamics in the static boundary case, this is a sufficient condition to observe unlimited energy growth when a time dependence on the boundary is introduced. The elliptical billiard is not described by the LRA conjecture. It is indeed integrable for the static boundary case presenting a separatrix curve separating two types of dynamical regime: libration and rotation. The introduction of time perturbation in the boundary makes the separatrix curve turn into a stochastic layer allowing the particle to undergo successive crossings from the rotation to libration regions [29–31], leading to an unlimited diffusion of energy.

A recent study [32] indicates that non-linear phenomena such as stickiness can act as a slowing mechanism of FA. In fact, the finite time trappings around the stability islands influence some transport properties, making the system locally less chaotic [33]. Such an influence of stickiness can be found in several models and applications in the literature [3, 4, 34–38]. In this paper we revisit the problem of a stadium-like billiard with oscillating circle arc boundaries, focusing on the analysis of the mechanism that produces the decay of energy, where many low energy orbits are observed to undergo reduction of energy to an apparently stable state. We argue for the existence of a critical resonance velocity where high initial velocities produce FA and low initial velocities do not experience the unlimited energy growth. Such decay is caused by the influence of sticky orbits with resonance around the stability islands. It leads the chaotic orbits to undergo temporary trapping around stability islands and then be captured by the fixed points. A statistical investigation is performed in order to quantify this phenomenon. A similar approach was used previously [39–44], but in this paper we emphasize the decay of the energy and the origin of this in stickiness for the first time. We also discuss the statistics of transport in the velocity axis near a resonant velocity

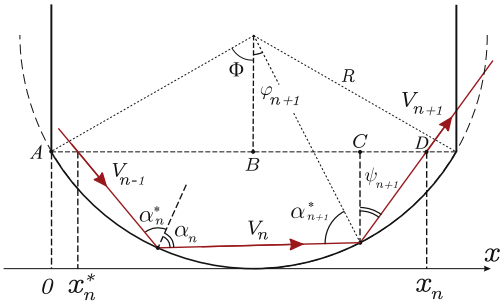

Figure 1. A sketch of the model near a focusing boundary featuring a typical trajectory undergoing successive collisions.

marking a separation of low energy to high energy regimes producing the decay of energy and the phenomenon of unlimited energy growth.

The paper is organized as follows. In section 2 we describe the dynamics of the stadium billiard and a study of its chaotic properties. Section 3 is devoted to the discussion of the statistical and transport analysis of the properties for both ensembles of initial conditions, considering the low and high energy regimes. Here we also present the influence of the stickiness orbits that hold the orbits in quasi-periodic motion near the fixed points, which causes the decay of energy. Finally, in section 4, our final remarks and conclusions are presented.

2. The stadium billiard as a model: mapping and chaotic properties

This section is devoted to discussing the model and the equations describing the dynamics. The model consists of a classical particle (or an ensemble of non-interacting particles) moving inside a closed domain of stadium-like shape. The stadium billiard is composed of two parallel lines connected by regions of negative curvature [45, 46]. In this paper we consider the boundary of the stadium to be described by three geometric control parameters: a, which is the width of the circle arc; b, which indicates the depth of the curvature; and l, which is the strength of the parallel lines. Additionally, we introduce a time dependence in the boundary. The dynamics of a particle for the static version of the billiard is characterized by a constancy in the energy. However the defocusing mechanism, as proposed originally by Bunimovich [45], is responsible for generating chaotic dynamics under the condition $(4bl/a^2) \approx (l/2R) > 1$ [46, 47], where R is the original radius of the Bunimovich stadium. According to the LRA conjecture, a chaotic dynamics is a sufficient condition to produce unlimited energy growth in the velocity of the particle when a time perturbation to the boundary is introduced. The unlimited diffusion in velocity generated by the collisions of a particle with a massive and time moving boundary is known in the literature as FA [25]. Robustness is not a characteristic of the phenomenon since inelastic collisions [48–51], as well as dissipation introduced by the drag type force [52, 53], suppresses unlimited diffusion.

As usual in the literature, the dynamics of the particle are modelled using non-linear mapping. We therefore take into account two distinct possibilities for the dynamics which include (i) successive collisions and (ii) indirect collisions. For case (i), the particle suffers successive collisions with the same focusing component while in (ii), after suffering a collision with a focusing boundary, the next collision of the particle is with the opposite focusing boundary. A schematic illustration of both collision cases can be found in figures 1 and 2. In

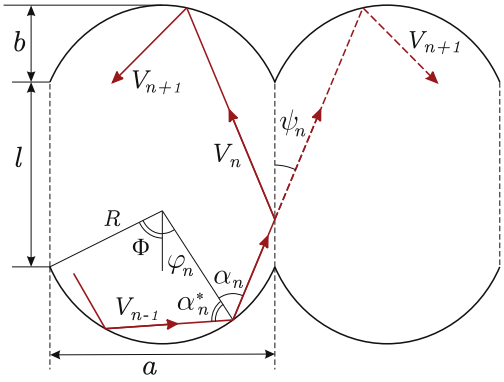

Figure 2. A sketch of indirect collision dynamics and its variables and parameters.

between such collisions the particle can, in principle, collide many times with the two parallel borders. We have considered that the time dependence in the boundary is $R(t) = R_0 + r\,\sin(wt)$, where $R_0 = (a^2 + 4b^2)/8b$ is the radius of the static boundary and $R_0 \gg r$. The definition of the parameters a and b can be found in figure 2. The velocity of the boundary is obtained by

$$\dot{R}(t) = B(t) = B_0 \cos(wt)\,, \tag{1}$$

where $B_0 = rw$ and r is the amplitude of oscillation of the moving boundary while w is the frequency of oscillation. In our investigation, however, we consider only the so called static boundary approximation (also called a simplified version). It assumes that the boundary is fixed, which makes the time spent between collisions easy to calculate. However, the velocity after a collision is calculated as if the boundary were moving. For this kind of approximation we may find some examples of dynamical systems whose behaviour is basically the same, considering the comparison between simplified and complete version dynamics. The bouncer model and standard map are two examples [32, 49, 50] and the stadium billiard itself [41, 42] shows a very similar dynamics for both versions.

The mapping is constructed for the variables α_n corresponding to the angle between the trajectory of the particle and the normal axis at the collision point, φ_n is the angle measured between the normal axis at the collision points and the symmetry line of the vertical axis of the stadium, t_n denotes the time and V_n the outgoing speed of the particle for the nth collision. The condition for observing case (i), i.e. successive collisions, is $|\varphi_{n+1}| < \Phi$, where $\Phi = \arcsin(a/2R_0)$ is the angle between the vertical symmetry line and the maximum angle of the negative curvature region. A typical successive collision case is shown in figure 1. Using basic geometry properties we obtain

$$\begin{cases} \alpha^*_{n+1} &= \alpha_n \\ \varphi_{n+1} &= \varphi_n + \pi - 2\alpha_n \pmod{2\pi} \\ t_{n+1} &= t_n + \frac{2R\cos(\alpha_n)}{V_n} \end{cases}, \tag{2}$$

where the superscript (*) represents the dynamical variable immediately before the collision.

Case (ii) is considered when $|\varphi_{n+1}| > \Phi$ and the particle collides with the opposite focusing component. In principle, the particle can suffer several collisions with the straight walls, so for such a collision, we make use of the unfolding method [26, 47] to describe the

dynamics. Two auxiliary variables are then introduced, ψ, which is the angle between the vertical line at the collision point and the particle's trajectory, and x_n, representing the projection over the horizontal axis. A sketch of indirect collisions is shown in figure 2. This leads to the following mapping

$$\begin{cases} \psi_n &= \alpha_n - \varphi_n \bmod (\pi/2) \\ x_n &= \frac{R}{\cos(\psi_n)}\left[\sin(\alpha_n) + \sin\left(\Phi - \psi_n\right)\right] \\ x_{n+1} &= x_n + l\tan(\psi_n) \bmod (a) \\ \alpha^*_{n+1} &= \arcsin\left[\sin\left(\psi_n + \Phi\right) - x_{n+1}\cos(\psi_n)/R\right] \\ \varphi_{n+1} &= \psi_n - \alpha^*_{n+1} \\ t_{n+1} &= t_n + \frac{R\left[\cos(\varphi_n) + \cos(\varphi_{n+1}) - 2\cos(\Phi)\right] + l}{V_n\cos(\psi_n)} \end{cases}. \tag{3}$$

The expression for the velocity of the particle after the collision is obtained by decomposing it into two separate components, which are

$$\begin{cases} \overrightarrow{v_n}\cdot\overrightarrow{T_n} &= v_n\sin\left(\alpha^*_n\right) \\ \overrightarrow{v_n}\cdot\overrightarrow{N_n} &= -v_n\cos\left(\alpha^*_n\right) \end{cases}, \tag{4}$$

where $\overrightarrow{T}$ and $\overrightarrow{N}$ are the tangent and normal unit vectors at the collision point. Because the collision is happening in a moving referential frame (non-inertial) we have to change the referential frame from inertial to non-inertial. The reflection law is then given by

$$\begin{cases} \overrightarrow{V}'_{n+1}\cdot\overrightarrow{N}_{n+1} &= -\kappa\overrightarrow{V}'_n\cdot\overrightarrow{N}_{n+1} \\ \overrightarrow{V}'_{n+1}\cdot\overrightarrow{T}_{n+1} &= \eta\overrightarrow{V}'_n\cdot\overrightarrow{T}_{n+1} \end{cases}, \tag{5}$$

where $\kappa \in [0, 1]$ and $\eta \in [0, 1]$ are the respective restitution coefficients for the normal and the tangent components, and the superscript $'$ resembles the non-inertial referential frame. In this paper we consider only the conservative case, therefore $\kappa = \eta = 1$, although the construction of the mapping is more general.

Returning to the inertial referential frame, the components of the velocity of the particle after collision are given by

$$\begin{cases} \overrightarrow{V}_{n+1}\cdot\overrightarrow{N}_{n+1} &= -\kappa\overrightarrow{V}_n\cdot\overrightarrow{N}_{n+1} + (1+\kappa)\overrightarrow{B}(t_{n+1})\cdot\overrightarrow{N}_{n+1} \\ \overrightarrow{V}_{n+1}\cdot\overrightarrow{T}_{n+1} &= \eta\overrightarrow{V}_n\cdot\overrightarrow{T}_{n+1} + (1-\eta)\overrightarrow{B}(t_{n+1})\cdot\overrightarrow{T}_{n+1} \end{cases} \tag{6}$$

Finally the velocity of the particle after the collision is given by

$$|\overrightarrow{V}_{n+1}| = \sqrt{\left(\overrightarrow{V}_{n+1}\cdot\overrightarrow{T}_{n+1}\right)^2 + \left(\overrightarrow{V}_{n+1}\cdot\overrightarrow{N}_{n+1}\right)^2}\ . \tag{7}$$

The two components of the velocity can be used to obtain the angle α, leading to

$$\alpha_n = \arcsin\left[\frac{|\overrightarrow{V_n}|}{|\overrightarrow{V_{n+1}}|}\sin\left(\alpha^*_n\right)\right]. \tag{8}$$

The dynamics of the particle is then evolved by considering equations (2), (3), (7) and (8) simultaneously.

3. Numerical results and statistical investigation

In this section we discuss how stickiness orbits influence the dynamics. Moreover, we take the study further by performing an extensive statistical investigation into the dynamics, in particular considering distributions of the angular variables along the dynamics. The novelty here is that after considering the histograms of frequency analysis for either the velocities or the polar angles for the decay of the velocity for a very long time series, we can see that the orbits, after experiencing the influence of stickiness, are captured by the fixed points, as if the dynamics was under the regime of dissipation. This makes the behaviour of the average velocity curves decay for lower energy ensembles. Also, a transport investigation is performed along the velocity axis considering both the low and high energy regimes in order to quantify the competition between the FA and the decay of energy near the critical resonance velocity.

3.1. Resonance velocity

Let us start by discussing the resonance velocity. The phase space may be represented, as is convenient, either using the angular coordinates $\alpha_{\rm n}$ and $\phi_{\rm n}$, or the auxiliary variables ψ and ξ, where $\xi = 0.5 + R_0 \sin(\phi_{n+1})/a$ is the projection along the horizontal axis and is usually normalized at mod (1). The fixed points ψ^* are deeply connected with $\alpha_{\rm n}$ because of the axial symmetry of the billiard. There is a sequence of fixed points corresponding to orbits always within the stadium at $\phi_n = 0$ (period-1), that intersects different multiples of the parameter a in the horizontal direction, according to the unfolding method [26, 47]. They are represented in the phase space by the elliptical stability islands in figure 3. Such stable orbits, can also be understood as librator-like trajectories inside the billiard (see [26] for details).

Considering the linearization of the unperturbed mapping [39–42] around the fixed points and according to the action-angle variables, one finds the rotation number $\sigma = \arccos\left(1 - \frac{8bl}{a^2\cos^2(\psi_n^*)}\right)$, where $\psi_n^* = \arctan(ma/l)$ is the fixed point and $m \geqslant 1$ is the number of mirrored *stadiums* that the particle can go through in a trajectory (for a detailed explanation see [40]).

Now, considering an orbit of a particle moving around a fixed point in the unperturbed (static) version of the billiard, the time spent between two successive collisions, i.e. the time between collisions with the two focusing components, is $\tau \approx \frac{l}{\cos(\psi_n^*)V_n}$ (considering the period-1 fixed point). Thus the rotation period of such an orbit around the fixed point is $T_{\rm rot} = \frac{2\pi\tau}{\sigma}$.

When a time perturbation is introduced in the focusing boundaries, there is an external perturbation period given by $T_{\rm ext} = \frac{2\pi}{w}$. When $T_{\rm rot} = T_{\rm ext}$ there is then a resonance between the moving boundary oscillations and the rotating orbits around the fixed points (see [40] for explanatory figures about this resonance). After grouping the terms properly one finds

$$V_r = \frac{wl}{\cos\left(\psi_n^*\right)\arccos\left(1 - \frac{8bl}{\left(a\cos\left(\psi_n^*\right)\right)^2}\right)}. \tag{9}$$

Of course, the value of V_r depends on which fixed point we are evaluating the linearisation. However, for all period-1 fixed points, one may found a very close value for the resonant velocity for all of them. For the combination of the parameters $l = 1.0$, $a = 0.5$,

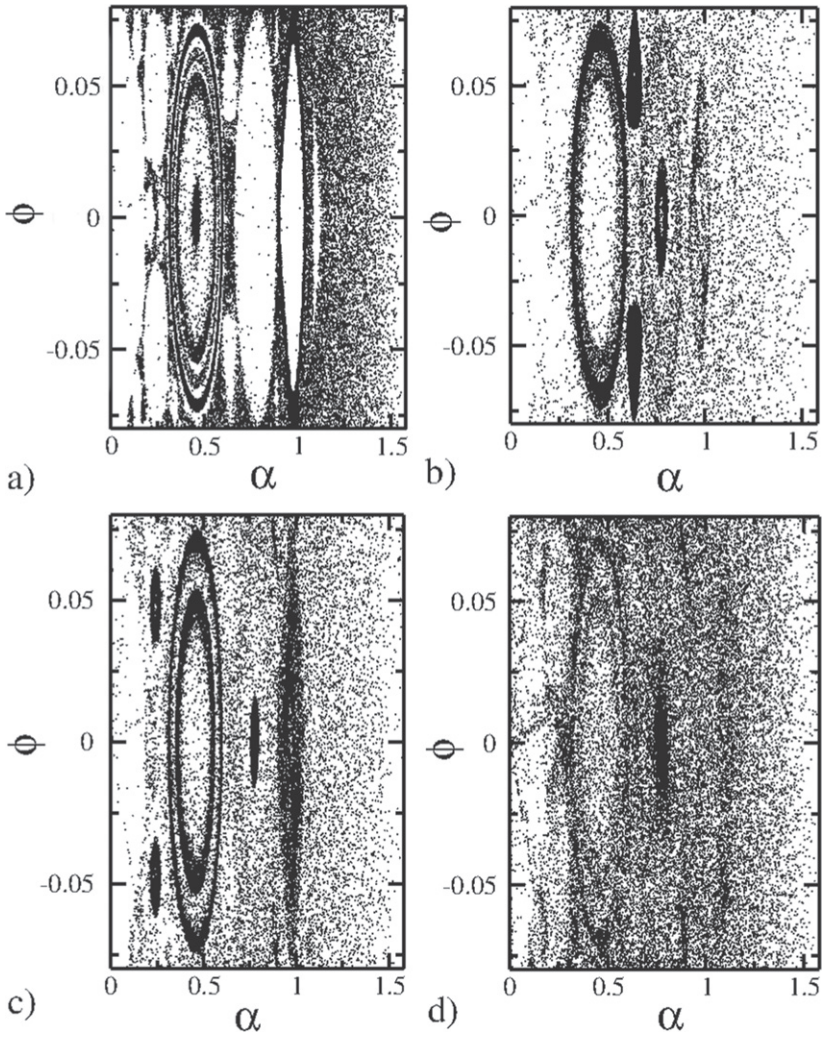

Figure 3. The phase space for the time-dependent stadium billiard. The initial velocities used were (a) $V_0 = 5$, (b) $V_0 = 1.5$, (c) $V_0 = 1.2$ and (d) $V_0 = 0.5$.

$b = 0.01$, we have $V_r = 1.2$, which is an average of all possible values for the different period-1 fixed points that one may find with the combination of the geometric control parameters given above. So, around V_r all the fixed points become resonant and increase the mixing in the phase space. For a better understanding of the influence of these parameters on the number of islands and fixed points in the phase space and their relation with the defocusing mechanism see [46, 47]. It must also be stressed that such a resonance is only observed when the defocusing mechanism is no longer active [46, 47], as with fully chaotic phase space no stability island exists, therefore no resonance is observed.

Indeed, resonance is a phenomenon often observed in dynamical systems with mixed phase space properties. When an orbit has a velocity equal to or less than the resonant velocity, the particle can penetrate into the neighbourhood of the fixed points. It may then enter the stability island for a while and the leave that region [2–4, 34], or it may be trapped in

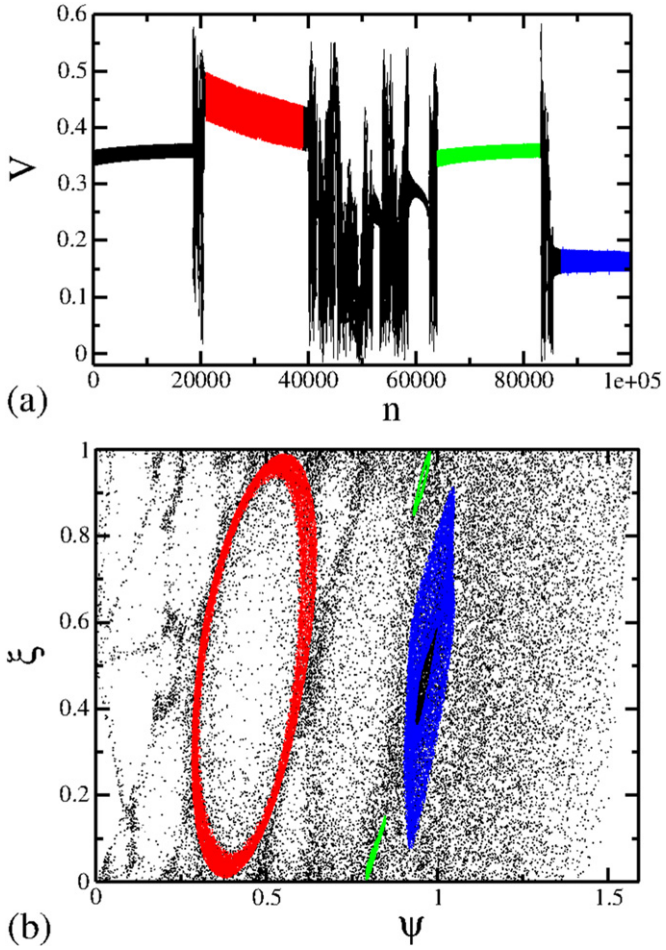

Figure 4. The influence of the stickiness orbits on the dynamics. (a) shows the evolution of the velocity as a function of the number of collisions and (b) shows the same orbit for the coordinates ψ and ξ. The initial velocity considered is $V_0 = 0.35$.

a pseudo-stable orbit for a long time. Such behaviour is as if it was attracted by the fixed point (we show this in the following sections). A possible explanation for this kind of phenomenon is related to the transformation of the invariant curve observed in the static version into a porous curve as the time perturbation is considered. Then a particle may cross a porous curve, which makes possible visits to previously forbidden regions which have now become accessible to the particle.

Figure 3 shows a phase space for different initial velocities considering both $V_0 < V_r$ and $V_0 > V_r$ for 25 different initial conditions chosen along the chaotic sea. As mentioned before, the phase space may be represented, as is convenient, either using the angular coordinates α_n and ϕ_n, or the auxiliary variables ψ and ξ. Figure 3 was constructed using α and ϕ for $\alpha \in [0, \pi/2]$ and $\phi \in [-\Phi, +\Phi]$. Stickiness regions can be seen in figure 3, particularly when the initial velocities are given close to but still below the resonant velocity. As the dynamics evolves, the orbits often change from an island to a surrounding region, leading to successive trappings and thus not allowing the velocity of the particle to reach higher values.

For sufficiently long times, the orbit chooses (the proper mechanism is not yet known) an island and stays there for very long time (as far we have studied, more then 10^9 collisions), as if it was attracted by the fixed point into a stable orbit. The temporary trapping around the stability islands is a possible reason to explain the decay of energy for an ensemble of low energies ($V_0 < V_r$), where many orbits are observed to undergo reduction of energy to an apparently stable state.

The mixed behaviour of the dynamics between the quasi-periodic and chaotic regions is shown in figure 4, where an orbit with an initial velocity lower than the resonant one is evolved for a long time, leading to temporary trappings as shown in figure 4(a), (b). A change in the coordinates of the phase space is made from polar angles (α, ϕ) to the auxiliary one (ψ, ξ), with $\xi = 0.5 + R_0 \sin(\phi_{n+1})/a$.

3.2. Statistical analysis

Let us start this section by discussing some statistical analysis concerning the behaviour of the average velocity. We consider the quadratic deviation of the average velocity as

$$\omega(n, V_0) = \frac{1}{M}\sum_{i=1}^{M}\sqrt{\overline{V_i^2}(n, V_0) - \overline{V}_i^2(n, V_0)}\ , \tag{10}$$

where M represents an ensemble of initial conditions. The average velocity is given by

$$\overline{V}(n, V_0) = \frac{1}{n}\sum_{i=1}^{n} V_i\ . \tag{11}$$

Figure 5 shows the evolution of different curves of ω as a function of n for different initial velocities. Each curve was constructed considering an ensemble of 2000 different initial conditions chosen along the chaotic sea. They were evolved in time up to 10^7 collisions with the boundary. One sees in figure 5(a) that all the initial velocities are lower than the resonant one ($V_0 < V_r$) and the ω curves stay constant for short times. After crossover, they experience decay for a long time series. On the other hand, figure 5(b) shows some curves of ω for initial velocities higher than the resonant one ($V_0 > V_r$). They initially present a constant plateau in the same range as their initial velocities and then suddenly bend towards a growth regime marked by a power law ($\omega \propto n^{\beta}$) with the exponent $\beta \approx 0.5$. The β exponent on the increments in the velocity variables is well described using a central limit theorem (CLT) [54, 55], so that over many time steps, the distribution of displacements is Gaussian with a variance exactly proportional to $\sqrt{n}$ leading to an unlimited growth in the velocity. It is important to emphasize that the curves of ω do not depend on the control parameters a, b and l, given that such parameters produce a behaviour which is scaling invariant [47]. Therefore, only one combination of the parameters is sufficient to show a tendency of the behaviour. The amplitude of the time perturbation is assumed to be constant, $B_0 = 0.01$, given that it is also scaling invariant [39].

As previously discussed and as is known in the literature, the high initial energy ensembles, those with an initial velocity higher than the resonant one, lead to FA [39, 40]. Therefore we will pay particular attention to the low energy ensemble, thus characterizing the decay of the energy mechanism and its correlation with stickiness orbits. As shown in figure 5, the separation of the ensembles is seen by considering the averages of different curves of ω. Because the average velocity is one of the observables responsible for characterizing the diffusion in energy, a statistical analysis with the average velocity for a grid of initial conditions is a natural and good procedure to quantify the dynamics, particularly the

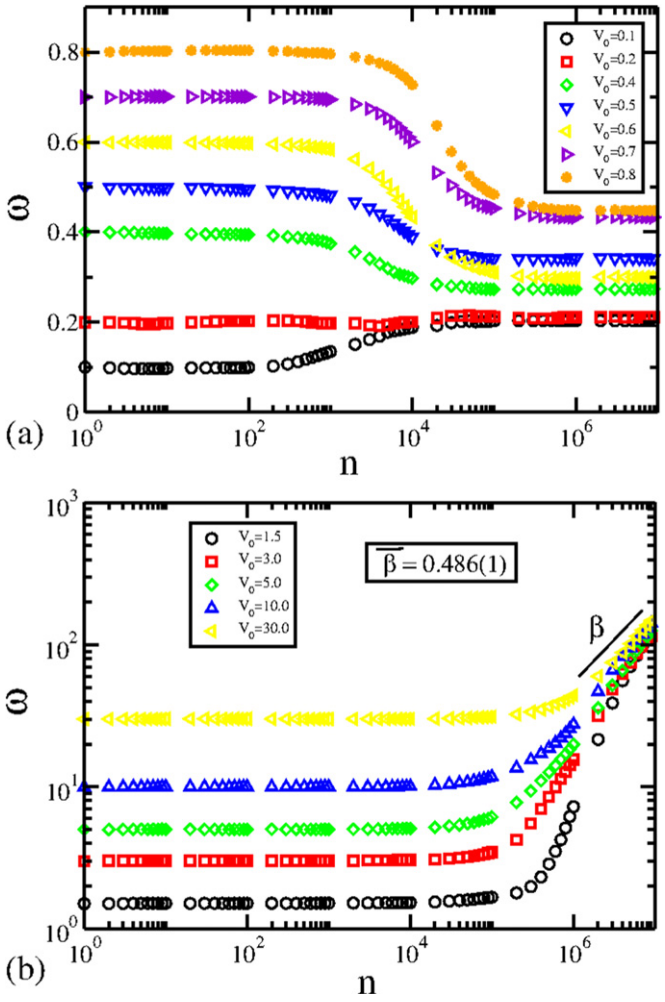

Figure 5. The behaviour of ω as a function of n for ensembles of low and high initial velocities. In (a) all curves experience a decay of energy caused by successive stickiness trappings while in (b) the curves experience a diffusion of energy leading to FA. They exhibit growth according a power law with the exponent $\beta \approx 0.5$ for long time. The initial velocities are labelled in the figure.

diffusion in energy. It allows us to see what initial conditions lead to the growth or decrease of the velocity, thus clearly defining which initial conditions produce Fermi acceleration. We then consider an investigation using the histograms of frequency technique, which lets us see which region in the phase space produces a larger stickiness, as shown in figure 6.

We then start considering the angular variables, i.e. the polar angles (α, ϕ). Since the stadium billiard has axial symmetry, the variable ϕ (or ξ) is not a good choice as it leads to an almost constant distribution along the dynamics. The same process is applied to the auxiliary variable ξ. We considered a set of 5×10^6 initial conditions chosen along the chaotic sea for both the ensembles of high and low energy. Each initial condition was iterated up to 10^7 collisions with the boundary. For the statistical process we collected and saved the final pair of angular variables at the end of this dynamical evolution. We see from figures 6(a)–(c) that

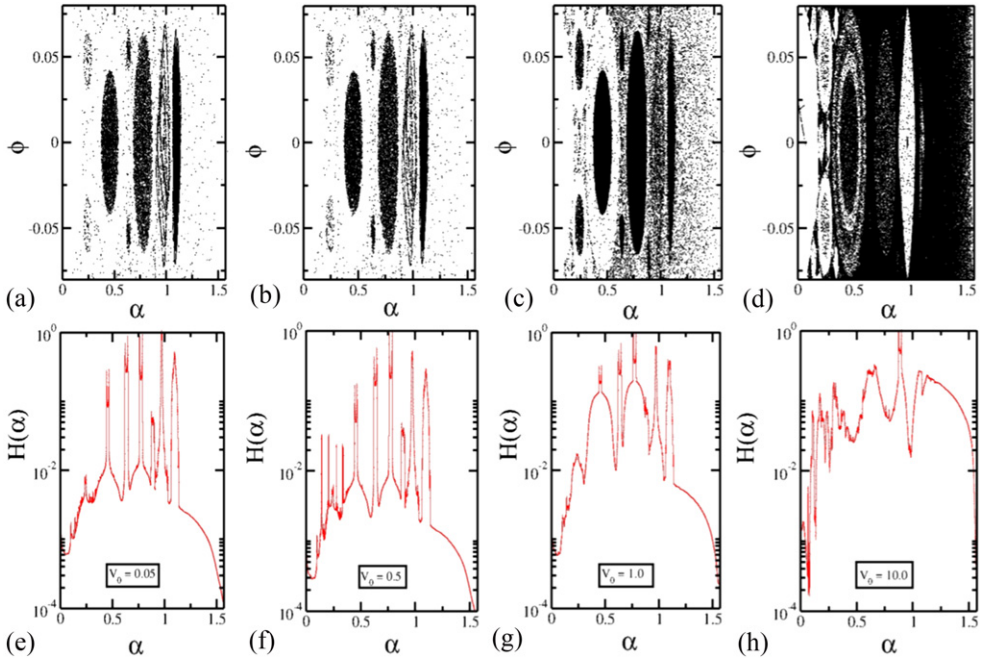

Figure 6. A comparison between the final pair of the angular coordinates (α, ϕ) for both low and high energy ensembles, with the frequency histogram along the whole dynamical evolution of the α coordinate. In (a) and (e) $V_0 = 0.05$, (b) and (f) $V_0 = 0.5$, (c) and (g) $V_0 = 1.0$, and (d) and (h) $V_0 = 10.0$. The histogram axes of (e), (f), (g) and (h) are plotted in the logarithmic scale.

for $V_0 < V_r$ the vast majority of points are located inside a stability island. Such a region is very close to where the fixed point is in the vicinity of the islands. This final behaviour indicates that the orbits are basically trapped inside the stability islands. Alternatively, they were attracted to their respective attracting fixed points, leading to clear evidence that the stickiness orbits are responsible for the decay of energy for initial velocities lower than the resonant one. To make a comparison, in figures 6(e)–(g) we have drawn the histograms of frequency for the whole evolution of the α variable along the dynamics for a set of initial conditions (10^6), but iterated to the same number of collisions and with the same initial velocity as figures 6(a)–(c). We can see some of the preferred regions for the variable α, which perfectly match the positions of the islands and the fixed points of figures 6(a)–(c). In particular, the shapes of the boundaries of the stability islands are well defined in the histogram of figure 6(g). The same procedure is performed, now considering the high energy ensemble, i.e. for $V_0 > V_r$, as shown in figure 6(d). One can see that there is no longer convergence of the final pair of angular variables to the regions of the stability islands and fixed points as seen previously. The final pair (α, ϕ) just remain wandering along the chaotic sea, a condition that explains why the orbits experience FA. The orbits for $V_0 > V_r$ also experience stickiness, as shown in figure 3(a). However, these trappings are not a sufficient condition to keep their velocity low. Also, in figure 6(h), we make a comparison with the whole distribution of the α variable along the whole dynamics, and we can see there is no longer any preferred region. In fact, the region in α concerning the chaotic sea shows a growth

in the histogram of frequency indicating high chaotic behaviour, therefore corroborating the FA phenomenon.

After a careful look at histogram of frequency, we can see that some islands are more preferred than others. This explains why, in figure 5(a), the decay of energy of the curves of ω produce several different plateaus of convergence for long times, which of course depend on the initial velocity. Each of the plateaus are related to the attraction of orbits to the periodic fixed points as shown in figure 6. The convergence plateaus are found in the finite region of $V_{final} \in (0.55, 0.15)$. In particular, the curve of ω for $V_0 = 0.1$ actually grows for this convergence region. Such a region seems to be the same concerning the convergence for final velocity when dissipation is acting in the system [56].

In an attempt to quantify the different plateaus of convergence, we made a histogram of the velocity distribution along the dynamics, considering the same ensemble as used to construct figure 6 and running the dynamics until 10^7 collisions. Figure 7(a) shows these distributions for three different values of initial velocities. One can see a major concentration for the low energy regime between 0.1 and 1.0. Several peaks are noted and a decrease in intensity as the initial velocity increases. Such behaviour is similar to the one shown in the zoomed inset in figure 7(a), even when $V_0 > V_r$, which is the case of $V_0 = 2.0$. Also, for initial velocities lower than the resonant one, there is a distribution for the velocity over V_r, which is not so intense for $V_0 = 0.05$ and $V_0 = 0.5$ and is quite significant for $V_0 = 2.0$. These distributions confirm what was assumed previously; not all initial conditions for $V_0 < V_r$ experience a decay of energy. In a complementary way, not all initial conditions with $V_0 > V_r$ lead to unlimited energy growth. Figure 7(b) shows the distribution of velocities for the lower energy regime as a comparison with their positions concerning the polar angular coordinate α. This comparison allow us to distinguish in which island of the phase space the orbits will converge for every range of final velocity plateaus. For example, a comparison between figures 7(a) and (b) shows higher intensity peaks for velocities between $V \approx 0.29$ and $V \approx 0.35$. They indicate the orbits prefer to stay in the last two period-1 islands of the phase space, i.e. those located near $\alpha \approx 0.97$ and $\alpha \approx 1.10$, respectively. Finally, for figure 7(c) we show the histogram of frequency for the high energy ensemble of initial velocities. Notice that the multiple peaks are no longer observed. Now we have a very well defined distribution along the velocities, meaning that for the very high energy ensemble, for example initial velocities at least ten times larger than V_r, FA is inherent in the system. Only very few orbits lead to a decay in energy, as shown by the green curve in figure 7(c) for $V_0 = 50$. We believe that the period-1 islands should be the preferred ones. All the results come from the resonance velocity, which marks the transition from the FA regime to the decay of energy. The analytical expressions were obtained considering the resonance around the period-1 islands. Also, they are the largest islands in the phase space, and show themselves to be more influential for the stickiness phenomenon. Different resonance velocities for different islands of different periods could be found, but even so the period-1 islands should be the more influential ones. Still, one thing that might change the preference between the islands would be a change in the value of the geometric control parameters. This change would influence the number of islands and also change the resonance velocity; see [39, 47].

3.3. Transport analysis

Let us now map along the phase space the initial conditions that lead to unlimited growth of energy and those producing the decay of energy. To start with, we consider an ensemble of initial conditions along the phase space uniformly distributed over α and ϕ assuming velocities either below $V_0 < V_r$ or above $V_0 > V_r$ to be resonant. We look at the time evolution of

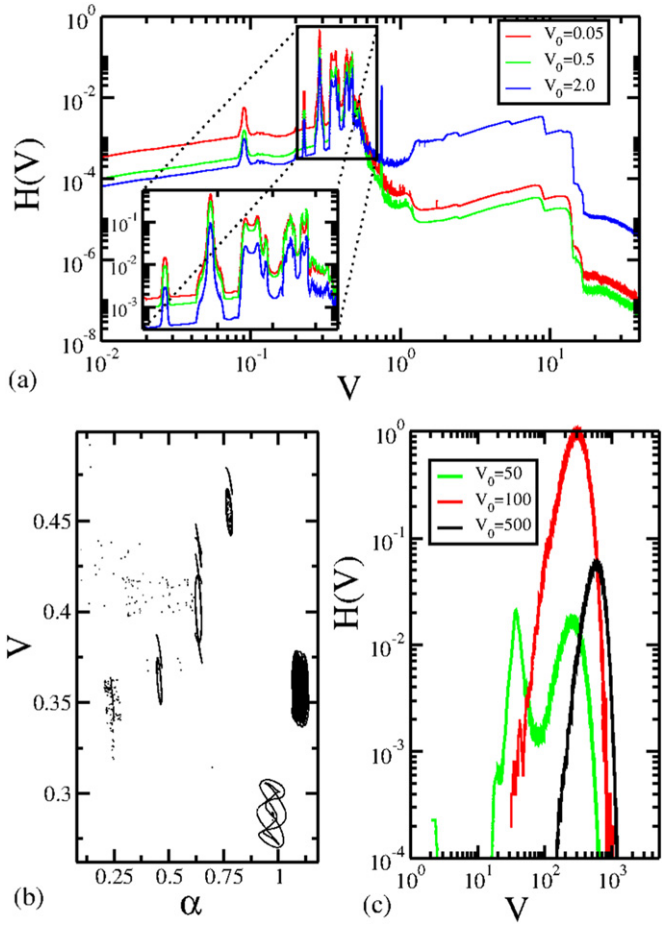

Figure 7. (a) The frequency histogram for the lower energy ensemble concerning the whole velocity distribution for $V_0 = 0.05$, $V_0 = 0.5$ and $V_0 = 2.0$. In particular, the zoomed inset shows the peaks of greatest intensity. (b) The convergence velocity as function of the α angle, where we are able to identify in which island the orbits were trapped and with which velocity. (c) The frequency histogram for the high energy ensemble, where the multiple peaks of intensity do not appear, and we have a very well defined distribution. The axes of (a) and (c) are in the logarithmic scale, for a better representation of their range and intensity.

each initial condition, then mapping those that cross the resonant velocity either coming from above, showing a decay of energy, or coming from below, therefore leading to unlimited energy growth.

Considering a distribution of initial conditions equally distributed in 2000 bins as $\alpha \in [0, \pi/2]$ and $\phi \in [-\Phi, +\Phi]$, we evaluated the dynamics considering the introduction of a hole in the system [57–61], placed concerning the resonance velocity $V_r = 1.2$. If an initial condition of $V_0 < V_r$ achieves sufficient energy to cross the resonant velocity we consider that it has escaped from the low energy region to a higher energy region. The same procedure applies to initial conditions in the high energy regime. So if it decays to a velocity smaller than V_r we consider that it has escaped from the high energy to lower energy region. We

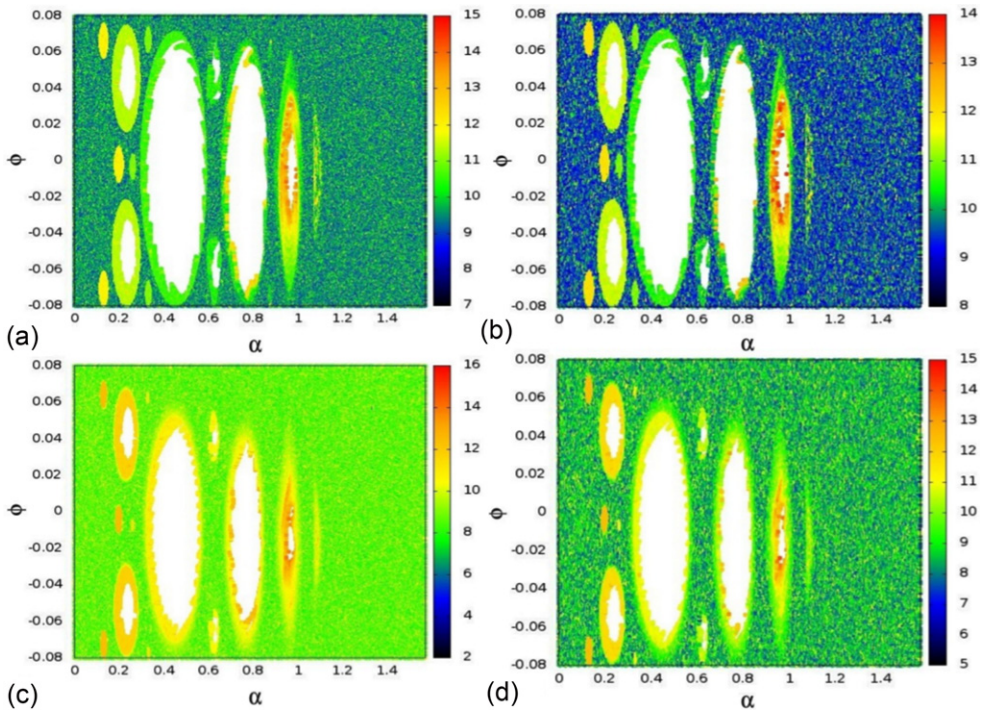

Figure 8. Transport analysis considering 'real escape' orbits. In (a) and (b) we have $V_0 = 2.0$, and in (c) and (d) we have $V_0 = 1.0$. The colour scale represents the escape collision. In (a) and (c) we have the initial conditions that crossed the resonance line and experienced FA, and in (b) and (d) we have the initial conditions that also crossed the resonance line, but experienced decay of energy. Note that the colour scale of all the figures is in the logarithmic scale for better representation of their intensity. Blue (black) indicates a fast escape, and yellow and red (grey and dark grey) represent long times for the orbit to escape. A white region means that the particle never escaped.

emphasize that multiple crossings from the same orbit can, in principle, happen, so we are only considering the first crossing with the V_r line, up to the maximum collision of 5×10^6.

Figure 8 shows a grid of initial conditions selected near the critical region leading to 'escape' using a colour scheme. figures 8(a)–(d) then represent in the colour scale the respective collision (in a log scale) where an initial condition has crossed the critical resonance velocity line for the first time. Blue (black) indicates fast escape, while yellow and red (grey and dark grey) denote long times until the orbit crosses the critical line. White regions mean that the orbits never escaped. One can see the existence of orbits trapped by stickiness near the islands of figures 8(a)–(d), indicated by yellow and red (grey and dark grey). Indeed, these quasi-periodic orbits produce a delay in the diffusion along the energy/velocity axis and hence in the escape through the resonant velocity, also leading to a delay in FA, and they are more numerous and influential for $V_0 < V_r$.

Considering first an initial velocity $V_0 = 2.0$, we marked the initial conditions that escaped and reached high velocities up to the end of the simulation in figure 8(a). In the same way the initial conditions that escaped and experienced decay of energy up to the end of the simulations are shown in figure 8(b). The same procedure was performed for an initial velocity $V_0 = 1.0$ and the initial conditions that escaped and acquired high velocities are

shown in figure 8(c) and, finally, the initial conditions that escaped but remained at the end of the dynamics under the influence of the decay of energy are shown in figure 8(d).

The percentages of the initial conditions of $V_0 = 2.0$ in figures 8(a), (b) are: 14.06% escaped and decreased their velocity up to the end of the simulations; 43.63% escaped and experienced FA; and 42.31% never crossed the critical line of resonance velocity. These results indicates that the vast majority of the initial conditions for $V_0 = 2.0$ remain in the high energy regime. Considering now the percentage of the initial conditions of $V_0 = 1.0$ in figures 8(c), (d), we found that: 55.41% of the initial conditions that escaped remained in the low energy regime up to the end of the simulations; 24.04% had escaped and experienced FA by the end of the simulations; and 20.55% never escaped. These results mean that for the initial conditions $V_0 = 1.0$, about 80% of the orbits stay confined in the lower energy regime. In particular, for all the items in figure 8, one can see a strong stickiness regime in the last two islands, which are the islands of main influence for the convergence of orbits, as shown in figure 7. This strong stickiness indicates that these orbits were trapped for very long times around that region and crossed the critical resonance line at a very late time, or did not even cross it, which can be taken as evidence that they were captured by the fixed points, which would lead to a reduction of their velocity.

4. Final remarks and conclusions

We revisited the problem of the time-dependent stadium-like billiard, aiming to understand and quantify the mechanism that is responsible for the decay of energy. A non-linear mapping was constructed, considering distinct kinds of collisions with the boundary to describe the dynamics. A resonance between the period of oscillation of the boundary and the rotation period around the fixed point was confirmed. Through this resonance, two ensemble regimes can be defined at low and high energy, where for high velocities FA is inherent.

A statistical and transport investigation along the phase space was performed concerning both regimes of initial energy as an attempt to describe the competition between the decay of energy and FA. We characterized the fundamental role of stickiness and initial conditions for the existence of FA.

Focusing on the lower energy regime, we have seen that stickiness orbits lead the velocity to decay. For long times the dynamics is stable when most of the orbits are located very close to the fixed points, where it seems that the orbits were captured by the fixed points, as if the dynamics was under the influence of dissipation and then suppression of the velocity. The results give support to new studies on the influence of stickiness in FA and diffusion processes, concerning systems with mixed properties in the phase space. It would also be interesting to investigate whether stickiness plays a similar role in other billiards and chaotic systems.

Acknowledgements

ALPL acknowledges CNPq and CAPES–Programa Ciências sem Fronteiras–CsF (0287-13-0) for financial support. MPS thanks FAPESP (2012/00556-6). IBL thanks FAPESP (2011/19296-1) and EDL thanks FAPESP (2012/23688-5), CNPq and CAPES, and Brazilian agencies. ALPL and MPS also thank the University of Bristol for kind hospitality during their stay in UK. This research was supported by resources supplied by the Center for Scientific Computing (NCC/GridUNESP) of the São Paulo State University (UNESP).

References

[1] Hilborn R C 1994 *Chaos and Nonlinear Dynamics: An Introduction for Scientists and Engineers* (New York: Oxford University Press)
[2] Lichtenberg A J and Lieberman M A 1992 *Regular and Chaotic Dynamics Applied Mathematical Sciences* vol 38 (New York: Springer Verlag)
[3] Zaslasvsky G M 2007 *Physics of Chaos in Hamiltonian Systems* (New York: Imperial College Press)
[4] Zaslasvsky G M 2008 *Hamiltonian Chaos and Fractional Dynamics* (New York: Oxford University Press)
[5] Scheneider J, Tél T and Neufeld Z 2002 *Phys. Rev.* E **66** 066218
[6] Portela J S E, Caldas I L and Viana R L 2011 *Int. J. Bifurcation Chaos* **17** 4067
[7] del-Castillo-Negrete D, Carreras B A and Lynch V E 2005 *Phys. Rev. Lett.* **94** 065003
[8] Jimenez G A and Jana S C 2007 *Composites* A **38** 983
[9] He P, Ma S and Fan T 2013 *Chaos* **22** 043151
[10] Andersen M F, Kaplan A, Grňzweig T and Davidson N 2006 *Phys. Rev. Lett.* **97** 104102
[11] Abraham N B and Firth W J 1990 *J. Opt. Soc. Am.* B **7** 951
[12] Milner V, Hanssen J L, Campbell W C and Raizen M G 2001 *Phys. Rev. Lett.* **86** 1514
[13] Tanner G and Søndergaard N 2007 *J. Phys. A: Math. Theor.* **40** 443
[14] Stein J and Støckmann H J 1992 *Phys. Rev. Lett.* **68** 2867
[15] Sirko L, Koch P M and Blümel R 1997 *Phys. Rev. Lett.* **78** 2940
[16] Haake F 2001 *Quantum Signatures of Chaos* (Berlin: Springer)
[17] Ponomarenko L A, Schedin F, Katsnelson M I, Yang R, Hill E W, Novoselov K S and Geim A K 2008 *Science* **320** 356
[18] Berggren K F, Yakimenko I I and Hakanen J 2010 *New J. Phys.* **12** 073005
[19] Jalabert R A, Stone A D and Alhassidd Y 1992 *Phys. Rev. Lett.* **68** 3468
[20] de Menezes D D, Jar e Silva M and de Aguiar F M 2007 *Chaos* **17** 023116
[21] Meza-Montes L and Ulloa S E 1997 *Phys. Rev.* E **55** R6319
[22] Xavier E P S, Santos M C, Dias da Silva L G G V, da Luz M G E and Beims M W 2004 *Physica* A **342** 377
[23] Oliveira H A, Manchein C and Beims M W 2008 *Phys. Rev.* E **78** 046208
[24] Zharnitsky V 1995 *Phys. Rev. Lett.* **75** 4393
[25] Fermi E 1949 *Phys. Rev.* **75** 1169
[26] Chernov N and Markarian R 2006 *Chaotic Billiards Mathematical Surveys and Monographs* vol 127 (Providence, RI: American Mathematical Society)
[27] Loskutov A, Ryabov A B and Akinshin L G 2000 *J. Phys. A: Math. Gen.* **33** 7973
[28] Loskutov A, Ryabov A B and Akinshin L G 1999 *J. Exp. Theor. Phys.* **89** 966
[29] Lenz F, Diakonos F K and Schmelcher P 2008 *Phys. Rev. Lett.* **100** 014103
[30] Lenz F, Petri C, Koch F R N, Diakonos F K and Schmelcher P 2009 *New J. Phys.* **11** 083035
[31] Leonel E D and Bunimovich L A 2010 *Phys. Rev. Lett.* **104** 224101
[32] Livorati A L P, Kroetz T, Dettmann C P, Caldas I L and Leonel E D 2012 *Phys. Rev.* E **86** 036203
[33] Manchein C, Beims M W and Rost J M 2014 *Physica* A **400** 186
[34] Bunimovich L A and Vela-Arevalo L V 2012 *Chaos* **22** 026103
[35] Zaslavsky G M and Edelman M 2005 *Phys. Rev.* E **72** 036204
[36] Szezech J D, Caldas I L, Lopes S R, Viana R L and Morrison J P 2009 *Chaos* **19** 43108
[37] Altmann E G, Motter A E and Kantz H 2006 *Phys. Rev.* E **73** 026207
[38] Custódio M S and Beims M W 2011 *Phys. Rev.* E **83** 056201
[39] Livorati A L P, Loskutov A and Leonel E D 2012 *Physica* A **391** 4756
[40] Loskutov A and Ryabov A B 2002 *J. Stat. Phys.* **108** 995
[41] Loskutov A, Ryabov A B and Leonel E D 2010 *Physica* A **389** 5408
[42] Ryabov A B and Loskutov A 2010 *J. Phys. A: Math. Theor.* **43** 125104
[43] Loskutov A and Ryabov A B 2001 *Int. J. Comput. Anticipatory Syst.* **8** 336
[44] Loskutov A, Akinshin L G and Sobolevsky A N 2011 *Appl. Nonlinear Dyn.* **9** 50
[45] Bunimovich L A 1979 *Commun. Math. Phys.* **65** 295
[46] Bunimovich L A 1991 *Chaos* **1** 187
[47] Livorati A L P, Loskutov A and Leonel E D 2011 *J. Phys. A: Math. Theor.* **44** 175102
[48] Leonel E D 2007 *J. Phys. A: Math. Theor.* **40** F1077
[49] Leonel E D and Livorati A L P 2008 *Physica.* A **387** 1155

[50] Livorati A L P, Ladeira D G and Leonel E D 2008 *Phys. Rev.* E **78** 056205
[51] Leonel D E and Marinho E P 2009 *Physica* A **388** 4927
[52] Tavares D F and Leonel E D 2008 *Braz. J. Phys.* **38** 58
[53] Tavares D F, Leonel E D and Costa Filho R N 2012 *Physica* A **391** 5366
[54] Adams W J 2009 *The Life and Times of the Central Limit Theorem* 2nd edn (Providence, RI: American Mathematical Society)
[55] Fischer H 2011 *History of the Central Limit Theorem* (New York: Springer)
[56] Livorati A L P, Caldas I L and Leonel E D 2012 *Chaos* **22** 026122
[57] Altmann E G, Portela J S E and Tél T 2013 *Rev. Mod. Phys.* **85** 869
[58] Leonel E D and Dettmann C P 2012 *Phys. Lett.* A **376** 1669
[59] Dettmann C P and Georgiou O 2011 *J. Phys. A: Math. Theor.* **44** 195102
[60] Dettmann C P and Georgiou O 2009 *Physica* D **238** 2395
[61] Dettmann C P and Leonel E D 2012 *Physica* D **241** 403